Eur. Phys. J. D **6**, 397–405 (1999)

THE EUROPEAN PHYSICAL JOURNAL D

EDP Sciences
© Società Italiana di Fisica
Springer-Verlag 1999

Reconstruction of the two-mode vibronic quantum state of a trapped atom

S. Wallentowitz[1,a], R.L. de Matos Filho[2], S.-C. Gou[3], and W. Vogel[1]

[1] Arbeitsgruppe Quantenoptik, Fachbereich Physik, Universität Rostock, Universitätsplatz 3, 18051 Rostock, Germany
[2] Instituto de Fisica, Universidade Federal do Rio de Janeiro, Caixa Postal 68528, 21945-970 Rio de Janeiro, RJ, Brasil
[3] Department of Physics, National Changhua University of Education, Changhua 50058, Taiwan

Received: 5 August 1998

Abstract. We present a method for the direct measurement of the Wigner-function matrix for complex vibronic states of a trapped atom, that is suited to analyse the entanglement between two motional degrees of freedom and the internal electronic dynamics. It is a generalisation of the method for the determination of vibronic quantum states [S. Wallentowitz, R.L. de Matos Filho, W. Vogel, Phys. Rev. A **56**, 1205 (1997)] in conjunction with the scheme for the direct observation of the Wigner function of a single motional degree of freedom [L.G. Lutterbach, L. Davidovich, Phys. Rev. Lett. **78**, 2547 (1997)]. The major advantage of the present method is that it reduces the experimental efforts substantially. On the other hand, it is demonstrated that the nonlinear vibronic coupling necessary for this method turns out to be its main limitation.

PACS. 03.65.Bz Foundations, theory of measurement, miscellaneous theories (including Aharonov-Bohm effect, Bell inequalities, Berry's phase) – 42.50.Vk Mechanical effects of light on atoms, molecules, electrons, and ions – 32.80.Pj Optical cooling of atoms; trapping

1 Introduction

Methods for reconstructing quantum states of light and matter nowadays are a subject of large interest [1]. The first experiments concerning quantum-state reconstruction have been performed with light pulses [2] and somewhat later the quantum state of a molecular vibration has been determined [3]. These approaches did apply methods of tomographic reconstruction [4], that require a (Radon) three-fold integral transform to reconstruct the Wigner function from measured data. Later on, the methods of quantum-state tomography have been further refined. The measured quadrature distribution could be directly related by a two-fold Fourier transform to the density matrix in a quadrature representation [5]. Alternatively, methods for the reconstruction of the density matrix in the number representation have been proposed [6,7] and experimentally realized [8].

Tomographic and other methods have also been proposed for reconstructing the motional quantum state of a trapped atom [9,10]. Quantum-state reconstruction methods for trapped atoms are of special importance in view of their outstanding feasibilities for preparing nonclassical quantum states of the atomic center-of-mass motion. In recent experiments, coherent states, number states, squeezed states, and Schrödinger-cat states have been prepared in the motion of a single trapped ion [11,12]. Moreover, there exist interesting possibilities to produce dark states of motion that are highly stable, including squeezed states, even and odd coherent states, nonlinear coherent states, pair coherent and pair cat states [13–15].

A significant reduction of the mathematical efforts to relate the quantum state of a bosonic mode to the measured data can be achieved by measuring its number statistics after introducing well-defined coherent displacements [16]. The quantum state is then obtained in the form of a quasiprobability distribution, as for example the Wigner function. Here the quasiprobabilities can be obtained as weighted sums of the measured number statistics, at phase-space points determined by the coherent displacements. Since the quasiprobabilities, which are locally determined at each phase-space point, are independent of those at other phase-space points, the method is not a tomographic but a local reconstruction method. Such a local method has been successfully applied in the experiment for the reconstruction of the motional quantum state of a trapped atom [17]. However, with a single trapped atom, quantum states having entangled external and internal degrees of freedom such as the Schrödinger-cat states, have been experimentally realised [12]. Moreover, there exist proposals to generate correlated states of two motional degrees of freedom [15] and also arbitrary entangled quantum states [18]. The full diagnostics of such

[a] e-mail: wal@physik3.uni-rostock.de

complex, entangled quantum states of a single trapped atom requires further extensions and improvements of the available methods.

For this purpose it is useful to consider the specific interaction dynamics of a trapped atom in some detail, including the internal and external atomic degrees of freedom and the driving lasers. In the resolved-sideband regime, this dynamics can be described by a nonlinear Jaynes-Cummings model [19]. In the particular case that the system is driven on resonance with a weak electronic transition, the interaction Hamiltonian does not alter the motional number statistics, while, due to its nonlinear character, it efficiently discriminates the different motional number states by phase shifts. Consequently, such a laser-atom interaction can be used for a quantum nondemolition measurement of the energy of the center-of-mass motion [20]. Moreover, this interaction can be used to reconstruct the full information on entangled vibronic quantum states from measured data [21], where the entangled vibronic quantum state describes the state of a motional and an electronic degree of freedom.

In a certain range of parameters [22], this laser-atom interaction has also been shown to allow one a direct mapping of the Wigner function of a single motional degree of freedom onto the electronic-state inversion [23]. Such a method directly yields the Wigner function as a measurable quantity and therefore would significantly reduce the set of required experimental data. Thus, it would be of vital interest to apply such a direct method for more complex, entangled quantum states, such as two-mode vibronic quantum states, for which the set of measurement data, required by conventional methods, would be very large.

In the present paper we show that the direct measurement of the Wigner function is practicable for quantum states of a trapped atom which is described by a two-level atom that undergoes a two-dimensional motion. For this purpose it is advantageous to extend the concept of the Wigner-function matrix used in reference [21] to include two motional modes. The direct measurement method is compared with a more involved QND-type reconstruction method. It will be shown that the limitations of both methods are strongly determined by the laser-induced, nonlinear vibronic coupling, with the QND-type method being of more general application.

The paper is organised as follows. First, in Section 2 the characterisation of the two-mode vibronic quantum states by an appropriate Wigner-function matrix is discussed. Then, in Section 3 we show that these quantities can be obtained from joint probabilities that are accessible in experiments by probing the electronic ground-state population. Here we study first the well established Raman-laser interaction and then two different measurement methods, namely a QND-based method and a direct measurement method. The limitations and the range of applicability of the proposed methods are considered in Section 4. Finally, a summary and some concluding remarks are given in Section 5.

2 Characterisation of the two-mode vibronic quantum state

In quantum theory the statistical properties of a quantum system with several degrees of freedom are usually characterised by the density operator $\hat{\varrho}$. For a single atom bound in an electromagnetic trap the degrees of freedom are given by the set of three coordinates x_i $(i=1,2,3)$ describing the center-of-mass motion in the direction of the principal axes of the trap and by the electronic degree of freedom.

2.1 Description for one motional degree of freedom

In many practical situations one is only interested in the dynamics of a single degree of freedom. Here it is of special interest to consider the motional degree of freedom of the atom describing its center-of-mass vibration along one principal axis of the trap, say x_1. This type of restricted information on the quantum state of the trapped atom is described by the reduced density operator $\hat{\rho}$ which is obtained by tracing over the remaining motional (x_2, x_3) and the electronic (el) degree of freedom,

$$\hat{\rho} = \mathrm{Tr}_{x_2,x_3}\mathrm{Tr}_{\mathrm{el}}\,\hat{\varrho}. \tag{1}$$

The calculation of expectation values of observables can be formulated similar to the classical probability theory by introducing quasiprobability distributions in the motional phase space, allowing one to use a phase-space description of the quantum state of the system. One prominent representative of these quasiprobability distributions is the Wigner function [24]. For a harmonic trap potential the Wigner function describing a single degree of freedom (in our case x_1) is given as [25]

$$W(\alpha) = \langle\, \hat{\delta}(\alpha-\hat{a})\,\rangle = \mathrm{Tr}\left[\hat{\rho}\,\hat{\delta}(\alpha-\hat{a})\right], \tag{2}$$

where the operator-valued delta function $\hat{\delta}(\alpha-\hat{a})$ is the Fourier transform of the coherent displacement operator,

$$\hat{D}(\alpha) = \exp(\alpha\hat{a}^\dagger - \alpha^*\hat{a}), \tag{3}$$

and can be given in the form [25]

$$\begin{aligned}\hat{\delta}(\alpha-\hat{a}) &= \frac{1}{\pi}\int \mathrm{d}^2\xi\,\hat{D}(\xi)\,e^{\alpha\,\xi^* - \alpha^*\xi} \\ &= \frac{2}{\pi}\,\hat{D}(\alpha)\,(-1)^{\hat{a}^\dagger\hat{a}}\,\hat{D}^\dagger(\alpha).\end{aligned} \tag{4}$$

In equations (3) and (4) $\hat{a}$ and $\hat{a}^\dagger$ are the bosonic annihilation and creation operators of vibrational quanta in the trap potential, respectively. The density operator can be obtained from the Wigner function by inverting equation (2),

$$\hat{\rho} = \int \mathrm{d}^2\alpha\, W(\alpha)\,\hat{\delta}(\alpha-\hat{a}), \tag{5}$$

so that the information on the quantum state contained in $W(\alpha)$ is equivalent to the information contained in the density operator $\hat{\rho}$. In order to reconstruct the reduced information on the quantum state describing the one-dimensional motion of a trapped atom, as given by the reduced density operator (1), several proposals have been made [9,10,23] and successful experiments have been performed [17].

2.2 Extension for two-mode vibronic quantum states

The Wigner function as given above cannot be used for dealing with systems having more than one degree of freedom. Thus, in order to have a complete description of a system with several degrees of freedom, one needs a more generalised definition for the quasiprobability distribution. A generalisation to include both the motional and electronic degree of freedom has recently been used in the context of a measurement scheme for reconstructing the complete information on the vibronic quantum state for a trapped atom [21].

For characterising more complex two-mode vibronic quantum states of a trapped atom we further extend the definition of the Wigner function to include two motional degrees of freedom x_1 and x_2 and the electronic degree of freedom by defining the two-mode Wigner-function matrix

$$\begin{aligned} W_{ij}(\alpha_1,\alpha_2) &:= \langle\, \hat{A}_{ji}\, \hat{\delta}(\alpha_1-\hat{a}_1)\, \hat{\delta}(\alpha_2-\hat{a}_2)\,\rangle \\ &= \mathrm{Tr}\left[\hat{\varrho}\, \hat{A}_{ji}\, \hat{\delta}(\alpha_1-\hat{a}_1)\, \hat{\delta}(\alpha_2-\hat{a}_2)\right]. \end{aligned} \quad (6)$$

Here $\hat{\varrho}$ is the jointed density operator describing the internal electronic and the two external motional degrees of freedom of the atom. The operators $\hat{a}_i$ and $\hat{a}_i^\dagger$ $(i=1,2)$ are the annihilation and creation operators of the center-of-mass motion along the principal axes x_i, respectively, and α_i are the complex-valued phase-space amplitudes of the two-dimensional motion. The electronic flip operator $\hat{A}_{ji} = |j\rangle\langle i|$ describes the transition from the electronic state $|i\rangle$ to the state $|j\rangle$.

Based on equations (4) and (6), by tracing over the electronic degree of freedom and using the cyclic property of the trace one obtains

$$\begin{aligned} &W_{ij}(\alpha_1,\alpha_2) = \\ &\frac{4}{\pi^2}\mathrm{Tr}\left[(-1)^{\hat{n}_1+\hat{n}_2}\hat{D}_1^\dagger(\alpha_1)\hat{D}_2^\dagger(\alpha_2)\hat{\varrho}_{ij}\hat{D}_1(\alpha_1)\hat{D}_2(\alpha_2)\right], \end{aligned} \quad (7)$$

where $\hat{\varrho}_{ij} = \langle i|\hat{\varrho}|j\rangle$ is an operator acting on the (two-mode) Hilbert space of the motional subsystem. Here $\hat{D}_i$ and $\hat{n}_i = \hat{a}_i^\dagger\hat{a}_i$ $(i=1,2)$ are the displacement operators and the numbers of vibrational quanta in the x_i mode, respectively. Performing the trace over the motional degrees of freedom, x_1 and x_2, with the help of the number states $\hat{n}_i|n\rangle_i = n|n\rangle_i$ $(i=1,2)$, we arrive at

$$W_{ij}(\underline{\alpha}) = \frac{4}{\pi^2}\sum_{m,n=0}^{\infty}(-1)^{m+n}\,\langle m,n|\,\hat{\varrho}_{ij}(-\underline{\alpha})\,|m,n\rangle, \quad (8)$$

where $|m,n\rangle = |m\rangle_1|n\rangle_2$ is a two-mode number state with m and n vibrational quanta in the modes x_1 and x_2, respectively, and total number of vibrational quanta $N=m+n$ [26]. Equation (8) relates the Wigner-function matrix at the phase-space point $\underline{\alpha}=(\alpha_1,\alpha_2)$ to the coherently displaced density operator

$$\hat{\varrho}_{ij}(-\underline{\alpha}) = \hat{D}_1^\dagger(\alpha_1)\,\hat{D}_2^\dagger(\alpha_2)\,\hat{\varrho}_{ij}\,\hat{D}_1(\alpha_1)\,\hat{D}_2(\alpha_2). \quad (9)$$

Note, that by inverting equation (6), the density operator of the whole vibronic quantum state can be obtained from the Wigner-function matrix as

$$\hat{\varrho} = \sum_{ij}\int\!\!\int \mathrm{d}^2\alpha_1\,\mathrm{d}^2\alpha_2\, W_{ij}(\underline{\alpha})\,\hat{A}_{ij}\,\hat{\delta}(\alpha_1-\hat{a}_1)\,\hat{\delta}(\alpha_2-\hat{a}_2), \quad (10)$$

showing that the Wigner-function matrix $W_{ij}(\underline{\alpha})$ contains the complete information on the two-mode vibronic quantum state of the trapped atom.

2.3 Properties of the Wigner-function matrix

In the following we will briefly discuss some properties of $W_{ij}(\underline{\alpha})$. First of all from equation (7) it can be seen that the Wigner-function matrix is Hermitian, that is $W_{ij}(\underline{\alpha}) = W_{ji}^*(\underline{\alpha})$. Moreover, the diagonal elements $W_{ii}(\underline{\alpha})$ represent the Wigner functions of the motional two-mode quantum states of the atom on condition that the electronic quantum state is in $|i\rangle$, whereas the off-diagonal elements $W_{ij}(\underline{\alpha})$ $(i\neq j)$ give information on the electronic coherence and the possible entanglement between motional and electronic degrees of freedom. Note that the elements of the Wigner-function matrix $W_{ij}(\underline{\alpha})$ are normalised to the corresponding elements of the reduced density matrix σ_{ij} of the electronic subsystem

$$\int\!\!\int \mathrm{d}^2\alpha_1\,\mathrm{d}^2\alpha_2\, W_{ij}(\underline{\alpha}) = \mathrm{Tr}\,\hat{\varrho}_{ij} = \sigma_{ij}. \quad (11)$$

In a similar way, taking the trace of the Wigner-function matrix over the electronic degree of freedom, one obtains the Wigner function corresponding to the reduced (two-mode) motional subsystem

$$W(\underline{\alpha}) = \sum_i W_{ii}(\underline{\alpha}). \quad (12)$$

Finally, if there exists no entanglement between the involved motional and electronic degrees of freedom of the trapped atom, the density operator of the system can be written as a direct product,

$$\hat{\varrho} = \hat{\sigma}\otimes\hat{\rho}_1\otimes\hat{\rho}_2, \quad (13)$$

where $\hat{\sigma}$ is the electronic density operator, and $\hat{\rho}_1$ and $\hat{\rho}_2$ are the density operators describing the motional quantum states of the modes in the x_1 and x_2 directions, respectively. In this case the corresponding Wigner-function matrix can be factorised to the form

$$W_{ij}(\underline{\alpha}) = \sigma_{ij}\, W_1(\alpha_1)\, W_2(\alpha_2), \quad (14)$$

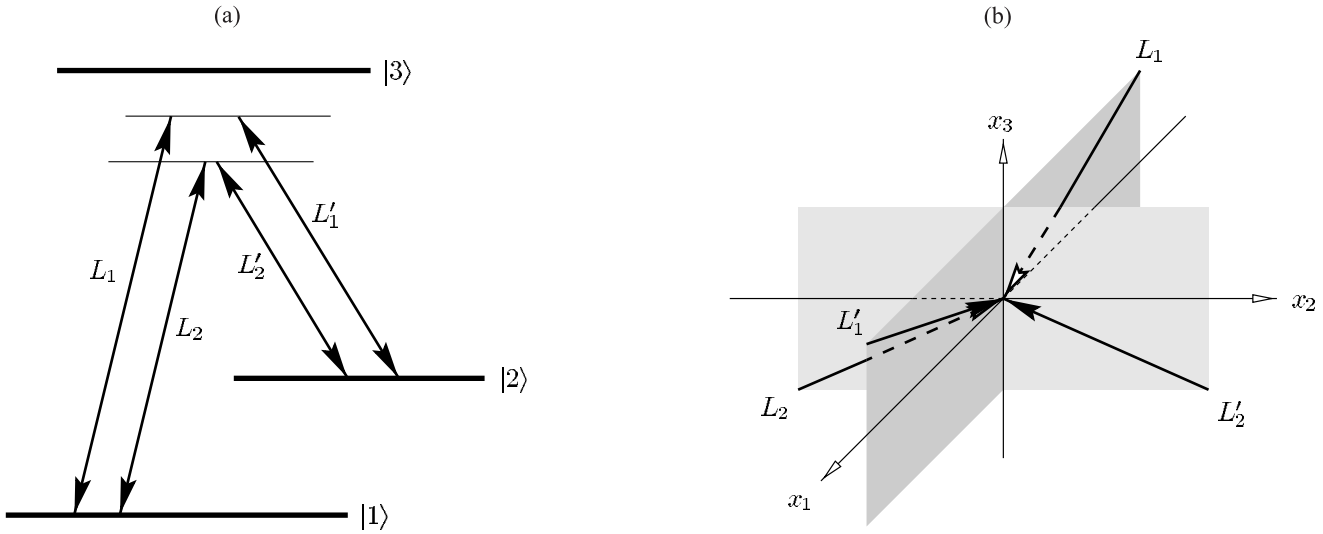

Fig. 1. (a) Three-level electronic system of the trapped atom for the measurement of the Wigner-function matrix. The weak electronic transition $|1\rangle \leftrightarrow |2\rangle$ is driven by two Raman-laser configurations (L_1, L_1' and L_2, L_2') and its inversion is tested by probing the strong transition $|1\rangle \leftrightarrow |3\rangle$ for resonance fluorescence. (b) The geometric setup of the four Raman-laser beams.

where $W_i(\alpha_i)$ are the Wigner functions corresponding to the density operators $\hat{\rho}_i$, showing the complete independence between the different degrees of freedom of the atom.

3 Determination of the Wigner-function matrix from measured data

In this section we will present two different schemes for the reconstruction of the Wigner-function matrix from measurements of the electronic state of the atom. While the first method relies on a QND-type measurement of the vibrational populations by a sequence of laser interactions intermitted by probing for fluorescence, the second method is largely simplified in that it gives one directly the value of Wigner-function matrix as a measurable joint probability of two no-fluorescence events. To proceed, let us first discuss the laser interaction that is needed for both types of methods.

3.1 Raman laser interaction

For measuring the Wigner-function matrix $W_{ij}(\underline{\alpha})$ we make use of a three-level electronic system as shown in Figure 1. The electronic transition of interest that mingles the motional degrees of freedom is the weak transition $|1\rangle \leftrightarrow |2\rangle$. This transition is simultaneously driven on resonance by two Raman-laser configurations with different detunings as shown in Figure 1(a). The Raman-laser fields are chosen to have wave vector differences which point into the x_1 (lasers L_1, L_1') and the x_2 (lasers L_2, L_2') directions, respectively, as depicted in Figure 1(b). The electronic dynamics of the weak transition $|1\rangle \leftrightarrow |2\rangle$ is monitored with very high quantum efficiency by probing the strong transition $|1\rangle \leftrightarrow |3\rangle$ for the appearance of resonance fluorescence [27]. That is, after a well-controlled interaction time of both Raman-laser configurations with the weak electronic transition, a laser pulse is applied on the strong transition. The appearance of fluorescence projects the atom into the electronic ground state $|1\rangle$ whereas the absence of fluorescence projects it into the excited electronic state $|2\rangle$.

For the weak transition being driven in the resolved-sideband limit and for different detunings of the two Raman laser pairs in x_1 and x_2 directions, we can generalise the results of [19] to two independently driven motional modes and obtain the interaction Hamiltonian (in vibrational rotating-wave approximation) as

$$\hat{H}_{\rm int} = \frac{1}{2}\,\hbar\left[\Omega_1 \hat{f}_0(\hat{n}_1;\eta_1) + \Omega_2 \hat{f}_0(\hat{n}_2;\eta_2)\right]\hat{A}_{21} + \text{h.c.} \quad (15)$$

Here Ω_i $(i = 1, 2)$ are the effective two-photon Rabi frequencies of the Raman laser pairs (L_i, L_i') driving the weak electronic transition and η_i are the Lamb-Dicke parameters characterising the spread of the atomic center-of-mass ground-state wave function with respect to the laser wavelengths of the beat notes of the Raman laser pairs in x_i directions.

The operator-valued function $\hat{f}_0(\hat{n};\eta)$ in equation (15) describes the nonlinearities in the vibronic coupling emerging from the interferences of the atomic center-of-mass wave function with the Raman laser pairs. It is given in its normally ordered form by

$$\begin{aligned}\hat{f}_0(\hat{a}^\dagger\hat{a};\eta) &= e^{-\eta^2/2}\sum_{k=0}^{\infty}(-1)^k\frac{\eta^{2k}}{(k!)^2}\,\hat{a}^{\dagger k}\hat{a}^k \\ &=: J_0\left(2\eta\sqrt{\hat{a}^\dagger\hat{a}}\right)\,e^{-\eta^2/2}:, \end{aligned} \quad (16)$$

where :: denotes normal ordering. In the following we choose the laser-beam geometry and the laser intensities such that the Lamb-Dicke parameters and the Rabi frequencies are equal for both Raman configurations, *i.e.* $\eta_1 = \eta_2 = \eta$ and $|\Omega_1| = |\Omega_2| = |\Omega|$ [28]. Accordingly, the interaction Hamiltonian reduces to

$$\hat{H}_{\rm int} = \frac{1}{2}\,\hbar\Omega\left[\hat{f}_0(\hat{n}_1;\eta)\,e^{i\varphi} + \hat{f}_0(\hat{n}_2;\eta)\,e^{-i\varphi}\right]\hat{A}_{21} + \text{h.c.}\,, \tag{17}$$

where $\varphi = \frac{1}{2}[\arg(\Omega_1) - \arg(\Omega_2)]$ is the phase difference of the two Raman-laser configurations which is chosen to be $\varphi = 0$ [29]. The phase of the Rabi frequency, $\Omega = |\Omega|\exp(i\phi)$, is given by

$$\phi = \frac{1}{2}\left[\arg(\Omega_1) + \arg(\Omega_2)\right], \tag{18}$$

and can be held very stable. Note, that the interaction Hamiltonian (17) fulfils the condition $[\hat{n}_i, \hat{H}_{\rm int}] = 0$ ($i = 1, 2$), so that the motional energy of the trapped atom is not changed by the laser interaction.

The time evolution of the density operator $\hat{\varrho}$ can be given in the interaction picture as

$$\hat{\varrho}(\tau) = \hat{U}(\tau - \tau')\,\hat{\varrho}(\tau')\,\hat{U}^{\dagger}(\tau - \tau'). \tag{19}$$

For notational simplicity we use here and in the following the dimensionless time

$$\tau = |\Omega| t, \tag{20}$$

which is scaled in units of electronic (Raman) Rabi cycles. The unitary time-evolution operator $\hat{U}(\tau)$ resulting from equation (17) is diagonal in the number-state representation with the diagonal elements given by

$$\langle m, n|\,\hat{U}(\tau)\,|m, n\rangle = \cos\left(\Omega_{mn}\tau\right) - i\sin\left(\Omega_{mn}\tau\right)\left(\hat{A}_{21}\,e^{i\phi} + \hat{A}_{12}\,e^{-i\phi}\right). \tag{21}$$

The coefficients Ω_{mn} describe the two-dimensional, nonlinear vibronic coupling which is due to interference effects between the Raman laser fields and the center-of-mass wave function of the trapped atom. They are known as the scaled, dimensionless Rabi frequencies of the two-mode vibronic interaction that can be explicitly expressed as

$$\Omega_{mn} = \frac{1}{2}\langle m, n|\left[\hat{f}_0(\hat{n}_1;\eta) + \hat{f}_0(\hat{n}_2;\eta)\right]|m, n\rangle = \frac{1}{2}\left[L_m(\eta^2) + L_n(\eta^2)\right]\,e^{-\eta^2/2}, \tag{22}$$

where $L_n(x)$ are the Laguerre polynomials. The behaviour of Ω_{mn} is shown in Figure 2.

The dynamics of the electronic transition $|1\rangle \leftrightarrow |2\rangle$ under the action of the Hamiltonian (17), as described by equation (21), allows one to determine the Wigner-function matrix $W_{ij}(\underline{\alpha})$ in two different ways. The first one consists in a QND-based measurement of each of the quantities $\langle m, n|\hat{\varrho}_{ij}(-\underline{\alpha})|m, n\rangle$ separately and the subsequent use of equation (8). The second one allows a direct measurement of $W_{ij}(\underline{\alpha})$ from joint probabilities.

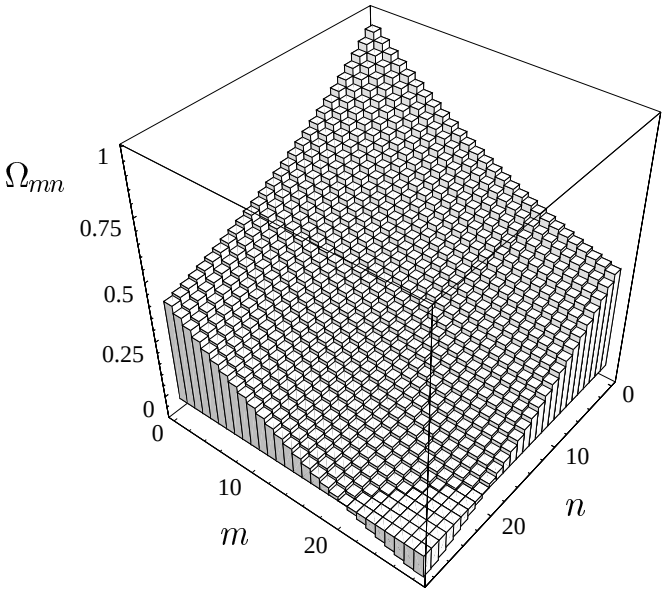

Fig. 2. Scaled Rabi frequencies Ω_{mn} plotted over m and n for $\eta = 0.25$. One clearly observes the zeros and the change of sign of the Rabi frequencies at $m, n \approx 20$.

3.2 Quantum nondemolition measurement method

Let us start with the QND-based method and suppose that before the ion interacts with the laser fields, the vibrations in x_1 and x_2 are coherently displaced by $-\alpha_1$ and $-\alpha_2$, respectively. This initial coherent displacement can be realized by applying radio-frequency fields to the ion, as has been demonstrated in the experimental determination of the quantum state of the motional subsystem [17]. If, after an interaction time τ_1 with the Raman laser fields, the atom is found in the excited electronic state $|2\rangle$, that is, no fluorescence has been observed during the excitation of the strong transition $|1\rangle \leftrightarrow |3\rangle$, the unnormalised density operator which is conditioned on this no-fluorescence events is given by

$$\hat{\varrho}(\tau_1) = |2\rangle\langle 2| \otimes \hat{\varrho}_{22}(\tau_1), \tag{23}$$

where the diagonal elements of the conditioned motional density operator $\hat{\varrho}_{22}(\tau_1)$ are determined by the unitary time evolution (21) as

$$\begin{aligned}\langle m, n|\hat{\varrho}_{22}(\tau_1;\phi)|m, n\rangle = {} & \\ \cos^2\left(\Omega_{mn}\tau_1\right)\langle m, n|\hat{\varrho}_{22}(-\underline{\alpha})|m, n\rangle & \\ + \sin^2\left(\Omega_{mn}\tau_1\right)\langle m, n|\hat{\varrho}_{11}(-\underline{\alpha})|m, n\rangle & \\ + \sin\left(2\Omega_{mn}\tau_1\right)\,\mathrm{Im}\left[\langle m, n|\hat{\varrho}_{12}(-\underline{\alpha})|m, n\rangle\,e^{i\phi}\right]. & \end{aligned} \tag{24}$$

Here the phase ϕ is a parameter yet to be determined.

Consider now k of such interaction-probe cycles with interaction times $\tau_1, \ldots, \tau_k$, each one accompanied by the absence of fluorescence. In this case the resulting conditioned motional number statistics after a sequence of k

cycles is given by

$$\langle m,n|\hat{\varrho}_{22}(\{\tau_l\};\phi)|m,n\rangle = \prod_{q=2}^{k}\cos^2\left(\Omega_{mn}\tau_q\right)\langle m,n|\hat{\varrho}_{22}(\tau_1;\phi)|m,n\rangle, \quad (25)$$

where $\{\tau_l\}$ denotes the set of k interaction times $\{\tau_l\}=\{\tau_k,\ldots,\tau_1\}$. The joint probability $P(\{\tau_l\};\phi)$ to obtain such a sequence of no-fluorescence events is then simply the trace of $\hat{\varrho}_{22}(\{\tau_l\};\phi)$,

$$P(\{\tau_l\};\phi)=\sum_{m,n=0}^{\infty}\langle m,n|\hat{\varrho}_{22}(\{\tau_l\};\phi)|m,n\rangle. \quad (26)$$

Our aim is to map the elements $\langle m_0,n_0|\hat{\varrho}_{ij}(-\underline{\alpha})|m_0,n_0\rangle$ onto the quantities $P(\{\tau_l\};\phi)$, which can be experimentally determined by the fraction of positive events in a large number of trials to obtain the above sequence of interaction-probe cycles. The first step consists in mapping pairs of elements with identical total numbers of quanta $N=m_0+n_0$,

$$\langle m_0,n_0|\hat{\varrho}_{22}(\tau_1;\phi)|m_0,n_0\rangle+\langle n_0,m_0|\hat{\varrho}_{22}(\tau_1;\phi)|n_0,m_0\rangle,$$

onto $P(\{\tau_l\};\phi)$ by choosing the interaction times $\tau_2,\ldots,\tau_k$ to be

$$\tau_2,\ldots,\tau_k=\frac{\pi}{|\Omega_{m_0n_0}|}\,p \qquad (p=1,2,\ldots), \quad (27)$$

where p can be different for each Raman-laser interaction. From equations (25) and (26) and the relation $\Omega_{mn}=\Omega_{nm}$ it can be seen that, after a sufficiently large number of interaction-probe cycles, $k\geq k_{\min}$, $P(\{\tau_l\};\phi)$ will converge to

$$P(\{\tau_l\};\phi)=\langle m_0,n_0|\hat{\varrho}_{22}(\tau_1;\phi)|m_0,n_0\rangle + \langle n_0,m_0|\hat{\varrho}_{22}(\tau_1;\phi)|n_0,m_0\rangle. \quad (28)$$

The first interaction time τ_1 and the phase ϕ can now be used to map the quantities $\langle m_0,n_0|\hat{\varrho}_{ij}(-\underline{\alpha})|m_0,n_0\rangle$ onto $\langle m_0,n_0|\hat{\varrho}_{22}(\tau_1;\phi)|m_0,n_0\rangle$ via equation (24). This is done by choosing three different interaction times, $\tau_1=T_{22},T_{11},T_{12}$, given by

$$T_{22}=0, \qquad T_{11}=\frac{\pi}{|\Omega_{m_0n_0}|}, \qquad T_{12}=\frac{\pi}{2|\Omega_{m_0n_0}|}. \quad (29)$$

Then for $\tau_1=T_{ij}$ we obtain a mapping onto the matrix element $\langle m_0,n_0|\hat{\varrho}_{ij}(-\underline{\alpha})|m_0,n_0\rangle$. For $\tau_1=T_{12}$ we additionally need two different laser phases $\phi=\pi/2$ and $\phi=0$ to obtain the real and imaginary part of $\langle m_0,n_0|\hat{\varrho}_{12}(-\underline{\alpha})|m_0,n_0\rangle$, respectively.

With this procedure one can obtain step by step the sum of elements given in equation (28) and one is able to reconstruct the Wigner-function matrix $W_{ij}(\underline{\alpha})$ by summing up the measured data according to equation (8). In the following we will concentrate on the measurement method which allows one to directly obtain the Wigner-function matrix as a joint probability for only two appropriately chosen Raman interaction times.

3.3 Direct measurement method

From equations (25) and (26) the joint probability for observing no-fluorescence events after only two Raman interactions with interaction times τ_1 and τ_2 results as

$$P(\{\tau_2,\tau_1\};\phi)=\sum_{m,n=0}^{\infty}\cos^2\left(\Omega_{mn}\tau_2\right)\langle m,n|\hat{\varrho}_{22}(\tau_1;\phi)|m,n\rangle = \frac{1}{2}+\frac{1}{2}\sum_{m,n=0}^{\infty}\cos\left(2\Omega_{mn}\tau_2\right)\langle m,n|\hat{\varrho}_{22}(\tau_1;\phi)|m,n\rangle. \quad (30)$$

Let us now consider the coefficients Ω_{mn} in more detail. From equation (22) we observe that the dependence on the motional quantum number n is determined by Laguerre polynomials $L_n(\eta^2)$. For small motional excitations the Laguerre polynomial may be expanded with respect to n,

$$L_n(\eta^2)=1-\eta^2 n+\mathcal{O}(\eta^4). \quad (31)$$

Inserting the expansion (31) into equation (22), the Rabi frequencies Ω_{mn} are approximated to be

$$\Omega_{mn}\approx\left[1-\frac{\eta^2}{2}\,(m+n)\right]e^{-\eta^2/2}. \quad (32)$$

To separate the motional part (cm) we choose the second interaction time to be $\tau_2=\tau_{\rm cm}$ with

$$\tau_{\rm cm}=\frac{\pi}{\eta^2}\,e^{\eta^2/2}. \quad (33)$$

Using the linear expansion (32) the occurring cosine in equation (30) reads

$$\cos\left(2\Omega_{mn}\tau_2\right)\approx\cos\left[\frac{2\pi}{\eta^2}\,e^{\eta^2/2}-\pi(m+n)\right] = C(\eta)\,(-1)^{m+n}, \quad (34)$$

with the constant $C(\eta)$ given by

$$C(\eta)=\cos\left(\frac{2\pi}{\eta^2}\,e^{\eta^2/2}\right). \quad (35)$$

The joint probability for observing two subsequent no-fluorescence events (30) then simplifies to

$$P(\{\tau_2=\tau_{\rm cm},\tau_1\};\phi)= \frac{1}{2}+\frac{C(\eta)}{2}\sum_{m,n=0}^{\infty}(-1)^{m+n}\langle m,n|\hat{\varrho}_{22}(\tau_1;\phi)|m,n\rangle. \quad (36)$$

We consider a Raman-laser configuration for the first interaction (interaction time τ_1) where the Lamb-Dicke parameter is very small so that we may operate in the Lamb-Dicke regime, affecting only the electronic populations but not the motional quantum state. This may be realized by applying two co-propagating Raman-laser beams to result in a minimal Lamb-Dicke parameter that is solely determined by the ratio of the vibrational frequencies to the frequency of the electronic transition $|1\rangle\leftrightarrow|2\rangle$. For this

case the relevant matrix elements of the density operator after the interaction time τ_1 read

$$\begin{aligned}\langle m,n|\hat{\varrho}_{22}(\tau_1;\phi)|m,n\rangle = \\ \cos^2\left(\frac{\tau_1}{2}\right)\langle m,n|\hat{\varrho}_{22}(-\underline{\alpha})|m,n\rangle \\ +\sin^2\left(\frac{\tau_1}{2}\right)\langle m,n|\hat{\varrho}_{11}(-\underline{\alpha})|m,n\rangle \\ +\sin(\tau_1)\,\mathrm{Im}\left[\langle m,n|\hat{\varrho}_{12}(-\underline{\alpha})|m,n\rangle e^{i\phi}\right]. \quad (37)\end{aligned}$$

As in the QND-based method we may now choose three different interaction times

$$T_{22}=0, \qquad T_{11}=\pi, \qquad T_{12}=\frac{\pi}{2}, \qquad (38)$$

such that $\tau_1 = T_{22}$, T_{11}, and T_{12} maps the matrix elements of the excited state, the ground state, and the electronic coherences onto $\langle m,n|\hat{\varrho}_{22}(\tau_1;\phi)|m,n\rangle$, respectively. For the choice $\tau_1 = T_{12}$ one again has to use two laser phases $\phi = \pi/2, 0$ to obtain the real and imaginary parts of the matrix elements of the electronic coherences. The relation between the joint probability (36) and the Wigner-function matrix elements finally reads

$$\begin{aligned}P(\{\tau_2=\tau_{\mathrm{cm}},\tau_1\};\phi) = \qquad (39)\\ \frac{1}{2}+\frac{C(\eta)}{2}\begin{cases} W_{11}(\underline{\alpha}), & \tau_1=T_{11},\\ W_{22}(\underline{\alpha}), & \tau_1=T_{22},\\ \mathrm{Re}\,W_{12}(\underline{\alpha}), & \tau_1=T_{12},\ \phi=\frac{\pi}{2},\\ \mathrm{Im}\,W_{12}(\underline{\alpha}), & \tau_1=T_{12},\ \phi=0.\end{cases}\end{aligned}$$

It is seen that the $W_{ij}(\underline{\alpha})$ is directly related to a measurable quantity, whereas in the QND method the Wigner-function matrix is obtained from a weighted sum over the measurable data.

4 Limitations of the reconstruction methods

Obviously, for both reconstruction methods there are limitations for their applicability which are due to the experimental parameters. Here especially the Lamb-Dicke parameter needed for the resonant vibronic laser interaction is of particular importance for the accuracy of reconstructed vibronic quantum states.

4.1 Limitations of the QND-based method

Let us first consider the limits of the applicability of the QND-based reconstruction method described in Section 3.2. This method relies on the ability to discriminate the number states $|m,n\rangle$ by the absolute values of their different (scaled) Rabi frequencies $|\Omega_{mn}|$. However, the Rabi frequencies Ω_{mn} given by the sum of two Laguerre polynomials (22) are in general not unique, so that for a given Lamb-Dicke parameter η, there may exist two different number states $|m,n\rangle$ and $|m',n'\rangle$ ($m'\neq n$, $n'\neq m$) for which $\Omega_{mn} = \pm\Omega_{m'n'}$. In other words, with increasing values of m,n the scaled two-mode Rabi frequencies

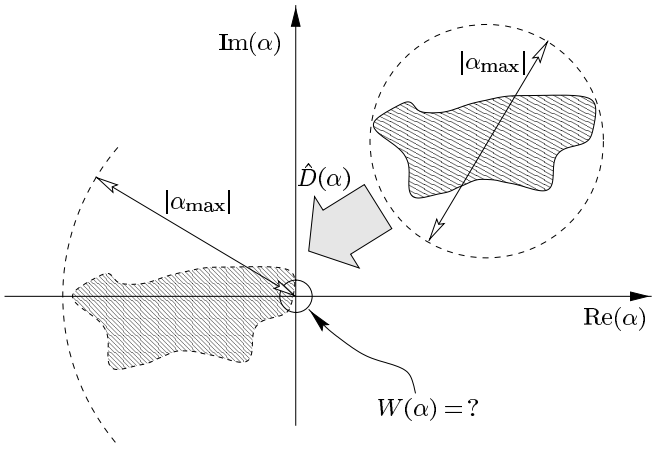

Fig. 3. Schematic determination of the maximum reconstructable quantum state for a single motional degree of freedom in phase space. The shaded areas represent the initial quantum state and the displaced state ($\hat{D}(\alpha)$, displacement amplitude α). The maximum phase-space extension of the initial quantum state $|\alpha_{\max}|$ determines the maximum amplitude of the displaced state for displacements α where the Wigner function $W(\alpha)$ is nonvanishing.

Ω_{mn} would decrease to zero and exhibit a change of sign at some value $m,n \approx n_{\max}$, leading to almost degenerate absolute values of the Rabi frequencies for the class of number states lower ($m,n<n_{\max}$) and the class of number states higher ($m,n>n_{\max}$) than the number $n_{\max}$ where the Rabi frequency vanishes. Therefore, to obtain a unique mapping of the absolute values of the Rabi frequencies $|\Omega_{mn}|$ onto the number states $|m,n\rangle$, the displaced number statistics has to be located below the excitation numbers m,n, where the Rabi frequencies Ω_{mn} vanish, that is $m,n<n_{\max}$. For example, in Figure 2 the "zeros" of the two-mode Rabi frequencies Ω_{mn} where the reconstruction will fail are clearly seen.

More quantitatively, the dependence of the maximum quantum number $n_{\max}$ on the Lamb-Dicke parameter, being determined by the first zero of the Laguerre polynomial (cf. Eq. (22)), can be approximately given by [30]

$$n_{\max} \approx \frac{9\pi^2}{64\eta^2}, \qquad (40)$$

so that for increasing Lamb-Dicke parameter the upper limit $n_{\max}$ decreases and the range of reconstructable quantum states becomes smaller.

Let us consider the vibrational quantum state whose Wigner function has in phase space some maximum extension $|\alpha_{\max}|$, see Figure 3. To reconstruct the complete phase-space distribution one therefore has to displace the initial state up to amplitudes of $|\alpha_{\max}|$. Therefore, the maximum absolute value of the amplitude of some phase-space components can be $|\alpha_{\max}|$ after the displacement, corresponding approximately to the number statistics with a tail at $|\alpha_{\max}|^2$. To obtain a good reconstruction of the Wigner function we have to request the

following relation

$$|\alpha_{\max}|^2 \approx n_{\max}, \tag{41}$$

where $n_{\max}$ is the maximum allowed number of vibrational quanta given by equation (40). Equation (41) gives a relation for the dependence of the maximum extension of the Wigner function on the Lamb-Dicke parameter

$$r_{\max} = \frac{3\pi}{8\eta} \approx \frac{1.2}{\eta}. \tag{42}$$

For the Lamb-Dicke parameter being $\eta = 0.1$, for example, the maximum extension in phase space is given by $|\alpha_{\max}| \approx 12$.

4.2 Limitations of the direct method

There also exist practical limits of the applicability for the direct measurement method. Since this method is based on a linear expansion of the vibronic two-mode Rabi frequencies in the vibrational quantum numbers, any higher-order term in the expansion of (22) has to be small compared with the linear term, that is for the expansion up to second order

$$L_n(\eta^2) \approx 1 - \eta^2 n \left[1 - \frac{1}{4}\,\eta^2(n-1)\right] + \mathcal{O}(\eta^6), \tag{43}$$

the second term in the bracket should be much smaller than the first one, *i.e.*

$$\frac{1}{4}\,\eta^2 n_{\max} \ll 1. \tag{44}$$

If we require the contribution of the quadratic term to the Rabi frequency to be a fraction p $(0 \le p \le 1)$ of that of the desired linear term, we obtain a relation for the maximum vibrational quantum number of the displaced number statistics,

$$n_{\max} \approx \frac{4}{\eta^2}\,p. \tag{45}$$

Compared with the limit for the QND-based method (40) this limit is more restrictive for reasonable values of the fraction p of the quadratic error. To reach the same range of applicability with the direct method as with the QND-based method, by equating (40) and (45), we get a value for the emerging fraction of quadratic errors in the direct method,

$$p = \frac{9\pi^2}{256} \approx 0.35. \tag{46}$$

That is, to obtain the same maximally reconstructable extension of the phase-space distribution one has to take into account a quadratic error in the Rabi frequencies of the order of 35%. Depending on the quantum state under study, these quadratic errors in the Rabi frequencies will decrease the quality of the reconstructed Wigner function.

We have now seen that the limitations of the range of reconstructable quantum states can be roughly given by a maximum phase-space extent $|\alpha_{\max}|$ which in general is larger for the QND-based reconstruction method. However, the direct method has the advantage of a reduced experimental effort, since only two laser pulses have to be applied for directly measuring the Wigner-function matrix as no-fluorescence joint probabilities, whereas for the QND-based method one usually needs several pulses to project the required displaced number statistics onto the measured signal.

5 Summary and conclusions

In conclusion we have proposed two related methods for determining the complete (possibly entangled) two-mode vibronic quantum state of a trapped atom. For the full characterisation of the electronic and motional degrees of freedom we use a Wigner-function matrix which combines the features of the two-mode motional Wigner function with those of the electronic density matrix. For the reconstruction from experimental data we have studied two schemes, that both rely on resonantly driving a weak electronic transition with two Raman-laser configurations and subsequently probing the electronic inversion with the help of laser-induced fluorescence on an auxiliary, strong electronic transition. The first method is based on the quantum nondemolition measurement of the motional statistics of the trapped atom: One has to project out the desired statistics by repeated application of interaction-probe cycles and sum it up to obtain the Wigner-function matrix elements at a phase-space point determined by the initial coherent displacement. In contrast to the QND-based method the direct method is largely simplified: It requires only two interaction-probe cycles, reducing the experimental efforts, and the Wigner-function matrix elements at the predefined phase-space points are directly measured as no-fluorescence joint probabilities. This advantage is accompanied by the restricted applicability of the direct method compared to the QND-based scheme, which is due to the nonlinear behaviour of the laser-induced vibronic coupling.

This research was supported by the Deutsche Forschungsgemeinschaft. S.-C. Gou is supported in part by the National Science Council, Taiwan, under Contract No. NSC-87-2112-M-018-009.

References

1. D.-G. Welsch, W. Vogel, T. Opatrný, to be published in Prog. Opt. **39**.
2. D.T. Smithey, M. Beck, M.G. Raymer, A. Faridani, Phys. Rev. Lett. **70**, 1244 (1993); D.T. Smithey, M. Beck, J. Cooper, M.G. Raymer, A. Faridani, Phys. Scr. **T48**, 35 (1993).
3. T.J. Dunn, I.A. Walmsley, S. Mukamel, Phys. Rev. Lett. **74**, 884 (1995).

4. K. Vogel, H. Risken, Phys. Rev. A **40**, 2847 (1989).
5. H. Kühn, D.-G. Welsch, W. Vogel, J. Mod. Opt. **41**, 1607 (1994); A. Zucchetti, W. Vogel, M. Tasche, D.-G. Welsch, Phys. Rev. A **54**, 1678 (1996).
6. G.M. D'Ariano, C. Macchiavello, M.G.A. Paris, Phys. Rev. A **50**, 4298 (1994); G.M. D'Ariano, U. Leonhardt, H. Paul, Phys. Rev. A **52**, R1801 (1995).
7. Th. Richter, Phys. Lett. A **211**, 327 (1996); U. Leonhardt, M. Munroe, T. Kiss, Th. Richter, M.G. Raymer, Opt. Commun. **127**, 144 (1996).
8. S. Schiller, G. Breitenbach, S. F. Pereira, T. Müller, J. Mlynek, Phys. Rev. Lett. **77**, 2933 (1996); G. Breitenbach, S. Schiller, J. Mlynek, Nature **387**, 471 (1997).
9. S. Wallentowitz, W. Vogel, Phys. Rev. Lett. **75**, 2932 (1995); Phys. Rev. A **54**, 3322 (1996); J.F. Poyatos, R. Walser, J.I. Cirac, P. Zoller, Phys. Rev. A **53**, R1966 (1996); C. D'Helon, G.J. Milburn, Phys. Rev. A **54**, R25 (1996).
10. For other nontomographic methods see P.J. Bardroff, C. Leichtle, G. Schrade, W.P. Schleich, Phys. Rev. Lett. **77**, 2198 (1996); M. Freyberger, Phys. Rev. A **55**, 4120 (1997).
11. D.M. Meekhof, C. Monroe, B.E. King, W.M. Itano, D.J. Wineland, Phys. Rev. Lett. **76**, 1796 (1996).
12. C. Monroe, D.M. Meekhof, B.E. King, D.J. Wineland, Science **272**, 1131 (1996).
13. J.I. Cirac, R. Blatt, A.S. Parkins, P. Zoller, Phys. Rev. Lett. **70**, 556 (1993).
14. R.L. de Matos Filho, W. Vogel, Phys. Rev. Lett. **76**, 608 (1996); Phys. Rev. A **54**, 4560 (1996).
15. S.-C. Gou, J. Steinbach, P.L. Knight, Phys. Rev. A **54**, R1014 (1996); Phys. Rev. A **54**, 4315 (1996); Phys. Rev. A **55**, 3719 (1997).
16. S. Wallentowitz, W. Vogel, Phys. Rev. A **53**, 4528 (1996); K. Banaszek, K. Wódkiewicz, Phys. Rev. Lett. **76**, 4344 (1996).
17. D. Leibfried, D.M. Meekhof, B.E. King, C. Monroe, W.M. Itano, D.J. Wineland, Phys. Rev. Lett. **77**, 4281 (1996).
18. B. Kneer, C.K. Law, Phys. Rev. A **57**, 2096 (1998); G. Drobný, B. Hladky, V. Buźek (unpublished).
19. W. Vogel, R.L. de Matos Filho, Phys. Rev. A **52**, 4214 (1995).
20. R.L. de Matos Filho, W. Vogel, Phys. Rev. Lett. **76**, 4520 (1996); L. Davidovich, M. Orszag, N. Zagury, Phys. Rev. A **54**, 5118 (1996); F.E. Harrison, A.S. Parkins, M.J. Collett, D.F. Walls, Phys. Rev. A **55**, 4412 (1997).
21. S. Wallentowitz, R.L. de Matos Filho, W. Vogel, Phys. Rev. A **56**, 1205 (1997).
22. For possibilities of extending the parameter range, see R.L. de Matos, W. Vogel, Phys. Rev. A **58**, R1661 (1998).
23. L.G. Lutterbach, L. Davidovich, Phys. Rev. Lett. **78**, 2547 (1997).
24. E.P. Wigner, Phys. Rev. **40**, 749 (1932).
25. K.E. Cahill, R.J. Glauber, Phys. Rev. **177**, 1882 (1969).
26. Note that the order of the arguments of the ket (bra) $|m,n\rangle = |m\rangle_1|n\rangle_2$ ($\langle m,n| = {}_1\langle m|_2\langle n|$) determines the degrees of freedom x_1 x_2.
27. W. Nagourney, J. Sandberg, H.G. Dehmelt, Phys. Rev. Lett. **56**, 2797 (1986); Th. Sauter, W. Neuhauser, R. Blatt, P.E. Toschek, Phys. Rev. Lett. **57**, 1696 (1986); J.C. Bergquist, R.G. Hulet, W.M. Itano, D.J. Wineland, Phys. Rev. Lett. **57**, 1699 (1986).
28. The Lamb-Dicke parameters and Rabi frequencies may be measured and adjusted by switching off one of the laser pairs in order to measure the Rabi oscillations in the population of the electronic ground state [11] for the coupling with the x_1 and x_2 modes separately.
29. The situation $\varphi = 0(\pi)$ can be reached by laser cooling the atomic motion to the ground state and adjusting the difference phase φ for observing the maximum Rabi frequency.
30. See equations (9.5.12) and (22.16.8) in M. Abramowitz, I.A. Stegun, *Handbook of Mathematical Functions* (Dover Publications, New York, 1972).